Cultural transmission of reproductive success impacts genomic diversity, coalescent tree topologies and demographic inferences

Jérémy Guez, Guillaume Achaz, François Bienvenu, Jean Cury, Bruno Toupance, Évelyne Heyer, Flora Jay, Frédéric Austerlitz

Cultural transmission of reproductive success impacts genomic diversity, coalescent tree topologies and demographic inferences

Jérémy Guez[1,2,*], Guillaume Achaz[1,3], François Bienvenu[4], Jean Cury[5], Bruno Toupance[1], Évelyne Heyer[1], Flora Jay[2,‡], and Frédéric Austerlitz[1,‡]

[1]UMR 7206 Eco-Anthropologie, CNRS, MNHN, Université Paris Cité, 75116, Paris, France
[2]Université Paris-Saclay, CNRS, INRIA, Laboratoire Interdisciplinaire des Sciences du Numérique, 91400, Orsay, France.
[3]SMILE group, Center for Interdisciplinary Research in Biology (CIRB), Collège de France, CNRS UMR 7241, INSERM U 1050, 75005, Paris, France
[4]Institute for Theoretical Studies, ETH Zürich, 8092, Zürich, Switzerland
[5]SEED, U1284, INSERM, Université Paris Cité, 75004, Paris, France
[‡]These authors contributed equally to this work.
[*]Corresponding author: jeremy.guez@outlook.fr

Abstract

Cultural transmission of reproductive success (CTRS) has been observed in many human populations as well as other animals. CTRS consists of a positive correlation of nongenetic origin between the progeny size of parents and children. This correlation can result from various factors, such as the social influence of parents on their children, the increase of children's survival through allocare from uncles and aunts, or the transmission of resources. Here, we study the evolution of genomic diversity over time under CTRS. CTRS has a threefold impact on population genetics: (1) the effective population size decreases when CTRS starts, mimicking a population contraction, and increases back to its original value when CTRS stops; (2) coalescent tree topologies are distorted under CTRS, with higher imbalance and a higher number of polytomies; and (3) branch lengths are reduced nonhomogenously, with a higher impact on older branches. Under long-lasting CTRS, the effective population size stabilizes but the distortion of tree topology and the nonhomogenous branch length reduction remain, yielding U-shaped site frequency spectra (SFS) under a constant population size. We show that this yields a bias in SFS-based demographic inference. Considering that CTRS was detected in numerous human and animal populations worldwide, one should be cautious because inferring population past histories from genomic data can be biased by this cultural process.

population genetics; evolution; cultural process; demographic inference; genetic diversity; coalescent tree shape; imbalanced topology

1 Introduction

In recent years, numerous studies have investigated the interactions between human culture and genetics. In some cases, cultural changes yield genetic adaptations. This was the case, for example, for lactase persistence that likely evolved independently in different human populations in Eurasia and Africa, due to the emergence of pastoralism (Swallow, 2003; Bersaglieri *et al.*, 2004; Tishkoff *et al.*, 2007; Gerbault *et al.*, 2011; Segurel *et al.*, 2020). Nevertheless, cultural processes can affect human genetic evolution without involving natural selection (Heyer *et al.*, 2012): (i) polygamy (including polyandry and polygyny), (ii) descent rules (patrilineal, matrilineal, or cognatic), and (iii) cultural transmission of reproductive success (CTRS).

CTRS is a positive correlation in the number of children between parents and children resulting from nongenetic causes. In that case, individuals with many siblings tend to have more children

than average. This transmission can result from multiple nongenetic causes: the social influence of parents on their children (Barber, 2001; de Valk, 2013; Kolk, 2014), the increase in child survival when uncles and aunts are present (allocare) (Heyer *et al.*, 2012; Lawson and Mace, 2011; Murphy, 2013) or the transmission of resources from parents to children. Such resources can be material resources (Sorokowski *et al.*, 2013), social resources (e.g., transmission of rank or of polygyny; Heyer *et al.*, 2012), or cultural resources (such as hunting skills; Mulder *et al.*, 2009). Furthermore, transmission of migration propensity across generations can have an effect similar to CTRS, with some lineages growing less than others due to their larger tendency to leave the population (Gagnon and Heyer, 2001; Gagnon *et al.*, 2006).

CTRS yields a decrease in effective population size and genetic diversity, and may increase the frequency of severe genetic disorders (Austerlitz and Heyer, 1998). The time to the most recent common ancestor is reduced, yet in a nonhomogenous way as the tree branches closer to the root are more strongly shortened (Sibert *et al.*, 2002). While these patterns can result from other evolutionary processes (e.g. bottlenecks, expansions), a more specific effect of CTRS is its impact on the topology of coalescent trees: CTRS yields imbalanced trees as it increases the proportion of lineages corresponding to large families (Sibert *et al.*, 2002). This specific property has been used in particular for inferring the transmission of reproductive success (TRS) on Y chromosome and mitochondrial DNA (Blum *et al.*, 2006; Heyer *et al.*, 2015). Since natural selection also implies a TRS, it is difficult to assess whether the imbalanced trees of nonrecombining uniparental markers result from natural selection or CTRS. Therefore, it is important to study the impact of CTRS on the nuclear genome. Recombination should indeed restrict the effects of natural selection to the genomic regions around selected loci (Li and Wiehe, 2013). Conversely, CTRS will yield an imbalance signal across the whole genome because in that case reproductive success is not linked to any locus in particular.

Studying the impact of CTRS on genomic diversity is particularly relevant, as it is a rather common phenomenon. Several demographic studies have shown a parents-children correlation in the number of children ranging generally between 0.1 and 0.25 (e.g., Murphy, 1999; Murphy and Wang, 2001; Gagnon and Heyer, 2001; Pluzhnikov *et al.*, 2007). There has been an extensive debate about whether these correlations result from cultural (Potter and Kantner, 1955; Duncan *et al.*, 1965) or genetic (Kohler *et al.*, 1999; Rodgers *et al.*, 2001; Mills and Tropf, 2015) transmission, the second case corresponding to natural selection. The correlations may, in fact, often be caused by both genetic and cultural transmission, along with interactions between genetics and the environment (Murphy, 2013), making the disentangling of those processes particularly difficult, especially as they can vary across populations and time. For instance, contemporary populations tend to have a stronger intergenerational correlation than populations that predate the demographic transition (Murphy, 1999; Murphy and Wang, 2001). Furthermore, this phenomenon is not limited to humans and has been described in various species such as hyenas (Engh *et al.*, 2000), Japanese macaques (Kawai, 1958), whales (Whitehead, 1998), dolphins (Frere *et al.*, 2010), and cheetahs (Kelly, 2001).

Another reason for studying the impact of CTRS on genomic diversity lies in its putative ability to impact summary statistics commonly used to infer other processes. For instance, site frequency spectra (SFS), which might be impacted by CTRS, are widely used for demographic inferences, either alone (e.g. $\delta a \delta i$ (Gutenkunst *et al.*, 2009), Fastsimcoal (Excoffier *et al.*, 2013), Stairway Plot (Liu and Fu, 2020), ABC-DL (Mondal *et al.*, 2019)) or jointly with other summary statistics (e.g., Sheehan and Song, 2016; Boitard *et al.*, 2016; Jay *et al.*, 2019; Terhorst *et al.*, 2017). These inference tools could thus be biased when applied to populations that have been affected by CTRS during part of their history. Understanding the interactions between CTRS and demographic changes is therefore relevant not only for inferring CTRS itself but also for improving demographic inferences, which is of broad interest (Beichman *et al.*, 2018).

This article pursues three objectives. First, we aim to improve our understanding of the impact of CTRS on nuclear genomes using simulations. Brandenburg *et al.* (2012) performed a simulation study that investigated the impact of CTRS on small sequences, ignoring intragenic recombination. Here, we study its impact on large recombining sequence data, adding numerous summary statistics not previously explored in CTRS scenarios. The summary statistics we assess are mainly of two kinds: (i) population genomic statistics, such as genetic diversity, Tajima's D and SFS, and (ii) various tree topology indices, such as tree imbalance indices and number of polytomies. In addition, we investigate the interaction of demographic changes and CTRS, as we expect human populations to undergo both types of processes. In particular, we look into the effect of an expansion occurring before and during

CTRS, an interaction that has not yet been explored. Second, we investigate the impact of CTRS duration and the persistence of ancient CTRS signals in the genome by measuring the evolution of the summary statistics over time (before, during, and after CTRS). In particular, this allows us to assess the impact of very short periods of CTRS on population genetics. Although long-lasting CTRS is not theoretically excluded, available anthropological evidence only indicates the presence of CTRS over short periods. For example, pedigrees from the Saguenay-Lac-Saint-Jean population show CTRS for 12 generations (Austerlitz and Heyer, 1998). For CTRS induced by variance in fertility among lineages within a population, the persistence of CTRS requires that individuals can trace back their lineage affiliation for several generations (in central Asia, Chaix *et al.* (2004) estimated this number of generations to be 7–10 depending on the population). Finally, we assess whether CTRS impacts demographic inference. For various CTRS scenarios, we compare the true and estimated instantaneous growth factor and timing of expansion.

2 Methods

2.1 Model

We implemented the CTRS model designed by Sibert *et al.* (2002) and Brandenburg *et al.* (2012) using the forward-in-time simulation framework SLiM (Haller and Messer, 2019). Individuals are diploid and monogamous, generations are nonoverlapping, and the population has a fixed number of individuals N with a 1:1 sex-ratio. At each generation, couples are formed uniformly at random before reproduction and never separated. One parental couple is randomly drawn from the population for each newborn child. This process is repeated until N offspring are produced. The probability p_i for a given couple i of being drawn for reproduction is given by:

$$p_i = \frac{\gamma_i(b) \times s_i^\alpha}{\sum_{j=1}^{N_c} \gamma_j(b) \times s_j^\alpha},$$

where s_i is the average sibship size of the two members of couple i, α is the parameter controlling the intensity of CTRS and b is the parameter controlling the variance in reproductive success. We denote N_c as the number of couples ($N_c = N/2$). The higher α is, the stronger the CTRS ($\alpha = 0$ means no CTRS, $\alpha = 2$ means a very strong CTRS). $\gamma_i(b)$ is a random gamma distributed variable drawn independently for each couple i, with shape parameter b and mean 1. Here, we considered only two cases: $b \to \infty$ (low variance in reproductive success, resulting in a Poisson-like distribution for the progeny size in the absence of CTRS, as $\lim_{b\to\infty} \gamma(b) = 1$) or $b = 1$ (high variance, resulting in a geometric-like distribution, as $\gamma(1)$ is an exponential of mean 1 distribution). Some results are shown for both values of b, but we focused mainly on the $b = 1$ case, as Austerlitz and Heyer (1998) found that the geometric-like model was more consistent with demographic data than the Poisson-like model and better explained the occurrence of genetic diseases in Saguenay-Lac-Saint-Jean.

For the demographic parameters, we compared two scenarios of constant population sizes (200 and 5000 individuals) and explored a scenario of sudden demographic expansion by a fivefold factor (200 to 1000 individuals). This expansion occurred 300 generations before the present.

2.2 Simulations

Unless specified otherwise, the simulations correspond to 200 replicates per scenario, a population size of 1000 individuals and a sample size of 30 individuals. Genomes were made of one chromosome of 10^7 bp in length, with a recombination rate and mutation rate of 10^{-8} per bp, which are commonly used parameters in human population modeling. We used the geometric-like model ($b = 1$) since Austerlitz and Heyer (1998) showed it was more realistic than the Poisson-like model ($b = \infty$) in the population of Saguenay-Lac-Saint-Jean where CTRS is documented from pedigree datasets. Coalescent trees are built in two steps: (1) forward-in-time simulations using our model implemented in SLiM (Haller and Messer, 2019) starting before the beginning of CTRS, resulting in trees that did not fully coalesce when the CTRS period is short, (2) a backward neutral coalescent process in order to complete the trees from the first step (i.e., to reach the most recent common ancestors throughout the genome). This step uses the *tskit* package functionality called *recapitation* (Kelleher *et al.*, 2016, 2019).

To assess the impact of CTRS on reproduction, we measured three demographic parameters : (1) the correlation between progeny sizes of all individuals and their parents' progeny sizes as a function of α, the strength of CTRS; (2) the variance of progeny size, and (3) the distribution of progeny sizes in the population for $\alpha = 0$, 1 and 2.

To investigate the effect of CTRS across time, we measured the genomic summary statistics on batches of individuals sampled through time for the following scenario: 2000 generations of CTRS, followed by 2000 generations with no CTRS. Every 50 generations, individuals were sampled for analysis. Following any cultural change (starting or stopping CTRS), we sampled more frequently to capture rapid fluctuations of summary statistics (at generations 2, 5, 10, 15, and 20 postchange).

2.3 Summary statistics

To assess the effects of CTRS on the genome, we explored the following diversity summary statistics as a function of time using the *tskit* package (Kelleher *et al.*, 2016, 2019): (1) the number of trees per chromosome, which is the number of recombination breakpoints plus 1, (2) the number of pairwise differences among the sampled chromosomes, (3) the average number of pairwise differences per tree, and (4) the number of SNPs in the chromosomes, (5) the average number of SNPs per tree, (6) Tajima's D, (7) the unfolded site frequency spectrum (SFS). For the SFS, we computed a transformed version (Lapierre *et al.*, 2017) that consists of multiplying singletons by 1, doubletons by 2, and n-tons by n. We then divided all bins by θ, which is estimated by taking the average of all bins so that the expected transformed SFS for the neutral case is a flat line with a value of 1.

We computed the theoretical effective size N_{exp} according to the equation $N_{\text{exp}} = 4N/(2 + s^2)$, where s^2 is the variance in progeny size (Wright, 1938; Ewens, 2016). This formula computes the effective size as a function of the census population size N and the variance in progeny size only. We compared N_{exp} to the observed effective size N_{obs} which was computed as follows: $N_{\text{obs}} = \theta/(4\mu L)$, with the average number of pairwise differences, $\hat{\theta}_\pi$, as an estimator of θ, L the genome length and μ the mutation rate per base pair.

We also computed various topology indices, to assess the effect of CTRS on the topology of coalescent trees, with the help of the *tskit* package (Kelleher *et al.*, 2016, 2019). Balance and imbalance indices: (1) I_b, the Brandenburg imbalance index (Brandenburg *et al.*, 2012; Blum *et al.*, 2006); (2) I_s^*, a normalized Sackin imbalance index (Sackin, 1972; Shao and Sokal, 1990); (3) I_{ce}^* and I_{ca}^*, two modified versions of the Colless imbalance index (Colless, 1982), ; (4) the B_1 balance index (Shao and Sokal, 1990); (5) the B_2 balance index (Shao and Sokal, 1990; Bienvenu *et al.*, 2021). Other topology indices: (1) the number of polytomies (nodes that have more than two direct children); (2) the number of interior nodes (all nodes excluding leaves and root). To compare different indices, we also used their standardized versions using their mean and standard deviation at generations preceding CTRS.

I_b, I_s^*, I_{ca}^* and I_{ce}^* measure the imbalance of trees, meaning that those indices take higher values for more imbalanced trees. I_b was computed using the script provided by Brandenburg *et al.* (2012). For one tree, I_b is the average of $I_{b,\text{node}}$ computed for each node in the tree according to the formula:

$$I_{b,\text{node}} = \frac{B - m_{s,l}}{D - m_{s,l}}, \text{ with } m_{s,l} = 2B_{s,l,\text{coal}} - D,$$

where s is the number of direct subnodes under the considered node and l the number of leaves descending from it. For each direct subnode under the considered node, leaves are counted and the maximum value is denoted B. D is the maximum value that B can possibly take (i.e., in the most imbalanced configuration) and is equal to $l - s + 1$. Thus, $\frac{B}{D}$ is the level of imbalance at this specific node. The correction factor $m_{s,l}$ enforces the expectation of I_b to be 0.5 for a standard population without CTRS. This parameter is evaluated based on simulations: $B_{s,l,\text{coal}}$ is the average B value of 1000 simulated random Kingman's (1982) incomplete coalescent trees with l leaves that were stopped when s parent nodes remained.

The Sackin imbalance index I_s is computed by counting for each leaf the number of nodes to reach the root and summing up all values. The Colless imbalance index I_c is computed by counting for each node (except for the root in our case) the difference in the number of leaves between its two children and summing up all values. However, this can be done only for binary trees. To handle polytomies, we designed two modified versions of the Colless imbalance index, I_{ce} and I_{ca}. For I_{ce}, the two children chosen for calculating the difference are those with the highest and lowest number of leaves (e, as for

extreme number of leaves). I_{ca} is computed by taking the average of differences for all pairs of children among all children of a given node (a, as for average). Since the Sackin and Colless indices minimum and maximum values depend on the number of nodes (Shao and Sokal, 1990) which varies across trees when permitting polytomies, we computed a corrected version of the Sackin (I_s^*) and Colless (I_{ce}^* and I_{ca}^*) indices which divides the index of each tree by the number of its interior nodes.

B_1 and B_2 are balance indices; we thus expect their value to be lower when trees are imbalanced. The B_1 balance index is computed by counting for each node the maximum path length to its leaves and taking the inverse of this value before summing up all of the values (one value per interior node). The B_2 balance index is based on p_k the probabilities to reach the leaf k assuming a random walk starting from the root and choosing a random direction at each node. B_2 is equal to the Shannon entropy of the p_k; a uniform distribution (an entropy of 1) corresponds to a balanced tree (Shao and Sokal, 1990; Bienvenu *et al.*, 2021).

Because of recombination, one chromosome corresponds to a sequence of coalescent trees. Summary statistics can be computed for each of the trees, with close trees having similar values. To consider the various histories represented by each of those trees, we explored not only the average summary statistics but also the shape of their distributions across the genome. The summary statistics were computed separately on each tree along the genome using the *tskit* package.

We also assessed the effect of sample size (number of individuals sampled) and of number of genomic regions on the power of detecting CTRS, using a Wilcoxon test with the significance threshold set to 0.01. For this assessment, we simulated 3,000 independent genomic regions of 1 Mb for two populations of 1000 individuals: one that went through a CTRS process of strength $\alpha = 1$ during 20 generations before present, and one with $\alpha = 0$ (no CTRS). We then sampled 5, 10, 30, 60, 90, and 120 diploid individuals from each of the two sets of 3,000 simulated regions and the four summary statistics (I_b, number of polytomies, B_1, and Tajima's D) on all of them (2 scenarios $\times$ 3,000 regions $\times$ 6 sample sizes $\times$ 4 summary statistics computations). For each sample size, we sampled $3, 4, 5, \ldots, 100$ regions from the two sets of 3,000 simulated regions, before using a Wilcoxon test to compare the four summary statistics values between the two populations ($\alpha = 0$ and $\alpha = 1$). For each combination of sample size and number of sampled replicates (6×98 combinations), the sampling among replicates and the Wilcoxon test were repeated 1000 times, with the proportion of P-values lower than or equal to 0.01 equaling the power of the test.

2.4 Assessing demography inference bias

To assess the bias in SFS-based demography inference, we used the software $\delta a \delta i$ (Gutenkunst *et al.*, 2009) with a one-event model. Two scenarios were studied: (1) a sudden fivefold expansion in population size that occurred 280 generations before a short period of CTRS (20 generations); and (2) a sudden fivefold expansion in population size that occurred during CTRS, after the first 1200 generations of a 1500-generations period of CTRS (Figure 1). We chose a fivefold sudden expansion as a simple illustration of a demographic event, which has the advantage of mimicking the past Neolithic expansion in human population history. From 30 diploid individuals sampled 300 generations after the demographic event, we inferred two parameters: the growth factor (expected value of 5) of the population and the number of generations since the event (expected value of 300 generations). The strength of CTRS was set to $\alpha = 1$. We compared the quality of inference in both scenarios to equivalent demographic scenarios without CTRS ($\alpha = 0$).

We inferred the parameters of 200 replicates for each of the four scenarios (scenarios 1 and 2 with $\alpha = 0$ or 1). Because the $\delta a \delta i$ optimization algorithm depends on the initialization of the model parameters, we repeated the inference three times for each replicate with different initialization values. We set the boundaries for the inferred growth factor at [0.01; 100] and for the inferred growth time at [0; 5] (time is expressed in $2N$ generations in $\delta a \delta i$, where N is the population size before the event). When the results were too close to the boundaries (> 99 or $< 1/99$ for the growth factor, > 4.9 or < 0.1 for the time since the event), the results were discarded. For each replicate, the remaining results among the three trials were kept, and their median was considered as the inferred parameter for this replicate. To convert time into generations, we multiplied the inferred time value of each replicate r by $2\hat{N}_r$; where $\hat{N}_r$ denotes the ancestral population size estimated for replicate r, using a $\hat{\theta}_r$ estimate computed by $\delta a \delta i$.

We removed outliers among replicates (i.e., values that were higher than $Q3 + 1.5 \times IQR$ and lower than $Q1 - 1.5 \times IQR$, with $Q3$ being the third quartile, $Q1$ being the first quartile and IQR being the

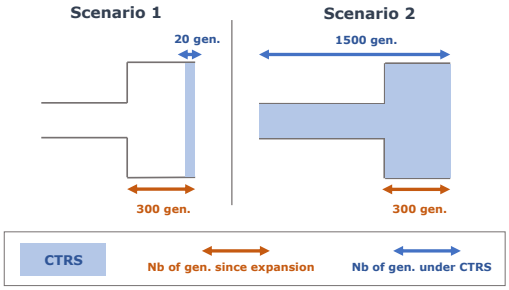

Figure 1: The two studied scenarios for SFS computation and $\delta a \delta i$ inference. In both scenarios, the expansion event occurs 300 generations before SFS computation and $\delta a \delta i$ inference. Scenario 1: 20 generations of CTRS before the present. Scenario 2: 1500 generations of CTRS before present.

interquartile range). We then computed the mean squared relative error (MSRE) and relative bias.

3 Results and discussion

3.1 Impact of CTRS on reproductive patterns

To assess the impact of CTRS on reproductive patterns, we simulated various strengths of CTRS (defined by α) for two models of variance in reproductive success (low variance with $b = \infty$ and high variance with $b = 1$). We computed the Pearson correlation coefficient between parents and children $\mathrm{Cor}_{P,C}$ and the variance and distribution of progeny size. As expected, $\mathrm{Cor}_{P,C}$ increases with α. However, this effect is weaker for smaller population sizes. This is due to an increased effect of stochastic processes in small populations, counteracting the impact of parents on children's progeny size (Figure 2a). The slope of the relationship between $\mathrm{Cor}_{P,C}$ and α is also lower for the $b = 1$ model than for the $b = \infty$ model (Figure 2a). Indeed, the higher variance in progeny size in the $b = 1$ model decreases the correlations, compared with the $b = \infty$ model.

Higher values of α yield more extreme progeny sizes (Figure 2b-C, purple compared with orange and green) and a higher variance (Supp. Fig. S1). This variance reaches a plateau after a few generations (Supp. Fig. S1). At this plateau, the exact progeny size distribution differs depending on the model: compared with the $b = \infty$ model, the $b = 1$ model yields a higher proportion of couples with no offspring and a lower proportion of couples with medium-sized families (1–3 children) (Figure 2b versus 2c).

3.2 Impact of CTRS on the genome

3.2.1 Effective population size

We then assessed the impact of CTRS on population genomic parameters. When CTRS begins, genomic diversity, measured either as the number of SNPs (Supp. Fig. S2a) or as the number of pairwise differences (Fig. 3a), declines and eventually reaches a plateau, showing a decrease in effective population size of 40 % for the $b = \infty$ model and of 75 % for the for the $b = 1$ model (for $\alpha = 1$, at the plateau), demonstrating a stronger effect of CTRS under the second model (Fig. 3b).

Because of this decrease in effective population size, the number of coalescent trees across the genome is lower due to fewer recombination events, and the TMRCA is smaller (Supp. Fig. S2b-C). For all these parameters, the plateau is lower for $\alpha = 2$, since it yields lower effective population sizes than $\alpha = 1$. Moreover, the higher α is, the faster the plateau is reached. This happens because genetic drift, which is stronger when α is high, swiftly erases past diversity. As soon as CTRS stops, diversity starts to increase slowly (Figure 3a), taking more time to recover than it took to decrease. Indeed, as the effective population size becomes larger, drift becomes weaker and the impact of past events lasts longer (i.e., diversity is close to equilibrium after $10N_e$ generations).

This decrease in effective population size results both from the increase in the variance of progeny size due to CTRS and the transmission of progeny size itself, which amplifies allele fixations by helping alleles carried by large lineages to spread faster in the population. To assess the respective impact of these two factors on effective population size, we compared N_{exp} (the expected effective population

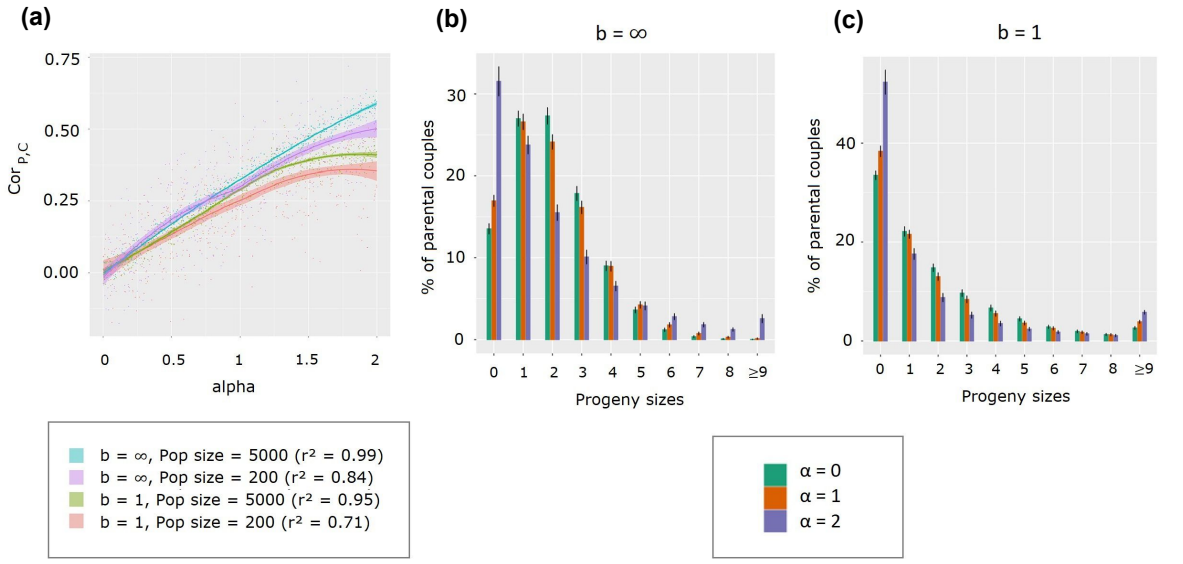

Figure 2: Impact of CTRS on two population reproduction variables. (a) Correlation between parents and children progeny size as a function of α, for four scenarios. In brackets: correlation between $\mathrm{Cor}_{P,C}$ and α for each scenario. Lines are drawn using locally weighted regression with the 95% confidence interval using the function loess of the R package ggplot2. (b) Distribution of progeny sizes for $\alpha = 0$ (green), 1 (orange) and 2 (purple), population size = 1000. The $b = \infty$ model is used (low variance of reproductive success). (c) Distribution of progeny sizes for $\alpha = 0$ (green), 1 (orange) and 2 (purple), population size = 1000. The $b = 1$ model is used (low variance of reproductive success).

size when taking into account the variance in progeny size only), to N_{obs} which is impacted by both components (Fig. 3b). We show that while a substantial decrease in effective population size is caused by the increased variance in progeny size, most of this decrease is due to the transmission component (around 70 % of the decrease in the $b = \infty$ model and 65 % of the decrease in the $b = 1$ model, for $\alpha = 1$).

3.2.2 Tajima's D

Tajima's D follows a more complex pattern than does genetic diversity. This pattern can be decomposed into four steps (Figure 4a): (1) as soon as CTRS begins, it increases rapidly towards a peak in positive values then (2) it decreases toward a plateau in negative values, (3) when CTRS stops, it rapidly decreases again toward more negative values, and (4) it slowly recovers to pre-CTRS levels. The first peak (1) results from a sudden decrease in effective population size when CTRS starts, as explained above, yielding a demographic contraction-like signal with positive values of D. Once this contraction signal is erased (i.e., the effective population size is still lower but there is no "memory" of the ancient effective population size due to an MRCA born after the change), D reaches a negative plateau at equilibrium; (2): the population is composed of many related individuals coming from large family lineages and few individuals from small family lineages, the latter yielding an excess of rare alleles. The nonhomogenous reduction of coalescent times, stronger for the branches closer to the root (Sibert *et al.*, 2002), also contributes to this excess of rare alleles. When CTRS stops, the decrease toward more negative values (3) is due to the increase in effective population size (expansion-like event). This negative peak is followed by a slow recovery (4) until the expansion signal is completely erased. These steps are not followed at the same pace along the genome: some coalescent trees will enter the equilibrium stage, while others retain a strong signal of the effective population size contraction, transiently yielding a bimodal distribution of D across the genome (Supp. Fig. S3b and C for $\alpha = 2$, Figure S3d for $\alpha = 1$).

Thus, understanding the effect of CTRS on Tajima's D requires accounting for three processes: changes in effective population size, an increased variance in relatedness among individuals as compared

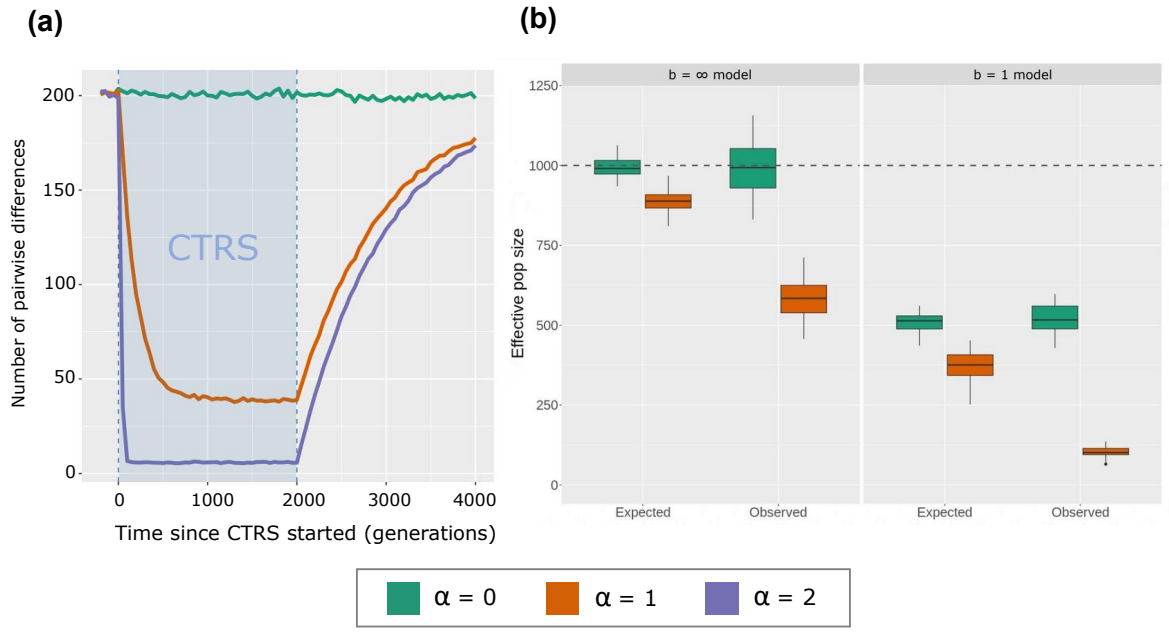

Figure 3: Factors of effective population size decrease under CTRS. (a) Average number of pairwise differences across time for three levels of CTRS: $\alpha = 0$, $\alpha = 1$ and $\alpha = 2$. In all cases, the $b = 1$ model of variance in progeny size is used. The blue rectangle corresponds to the period when populations are under CTRS. Generations are counted from the beginning of CTRS. (b) Expected effective population size given the observed offspring variance (N_{exp}) and observed effective population size measured using the number of pairwise differences at the plateau in Panel a as an estimator of θ (N_{obs}), for $\alpha = 0$ and $\alpha = 1$ and both models of variance in progeny size ($b = \infty$ and $b = 1$). The dotted line represents the census N value, which is 1000 individuals.

with a neutral population and a non homogeneous reduction in branch lengths. Timing is then an important factor: the relationship between α and Tajima's D changes over time after the beginning of CTRS, and the impact of CTRS on genetic diversity and D persists long after CTRS has stopped.

The interaction between demographic events and CTRS is also important, since both can happen in the same period of human history. When a fivefold expansion occurs during the equilibrium stage, Tajima's D decreases as expected, but the extent of this decrease depends on α: the stronger α is, the weaker the decrease will be, showing the nonadditivity of the two processes regarding D (Figure 4b, generation 1200). The recovery from the effect of this fivefold expansion also depends on α: when $\alpha = 1$, Tajima's D recovers faster than with no CTRS ($\alpha = 0$) (Figure 4b, generations 1,200 – 1,500). This is due to the smaller population effective size when $\alpha = 1$, which quickly erases past signals. Thus, we expect populations under CTRS to lose the genetic signals of past demographic events faster.

3.2.3 Coalescent tree topology

It is likely that neither diversity indices nor Tajima's D would be sufficient alone to infer CTRS in population genetics data, since demographic events also impact these statistics. In contrast, the shape of coalescent trees has been shown to display a CTRS-specific signal, with trees being more imbalanced only when CTRS is present, irrespective of the variation in total population size. Brandenburg *et al.*'s (2012) imbalance index I_b (Figure 5a) grows rapidly when CTRS starts and decreases as soon as it stops, recovering in a few dozens of generations, unlike Tajima's D (Figure 4a), which did not fully recover after $2N = 2000$ generations. The number of polytomies follows a pattern similar across time as I_b (Supp. Fig. S4). However, this increased number of polytomies can stem from the contraction in effective size yielded by CTRS (4-fold decrease when $\alpha = 1$ and $b = 1$), as coalescent rates are higher for smaller population sizes, increasing the probabilities of polytomies. To assess this hypothesis, we compared the number of polytomies after 500 generations of CTRS ($\alpha = 1$ and $b = 1$) to the number of polytomies after a 4-fold contraction 500 generations before the present, without CTRS. The results

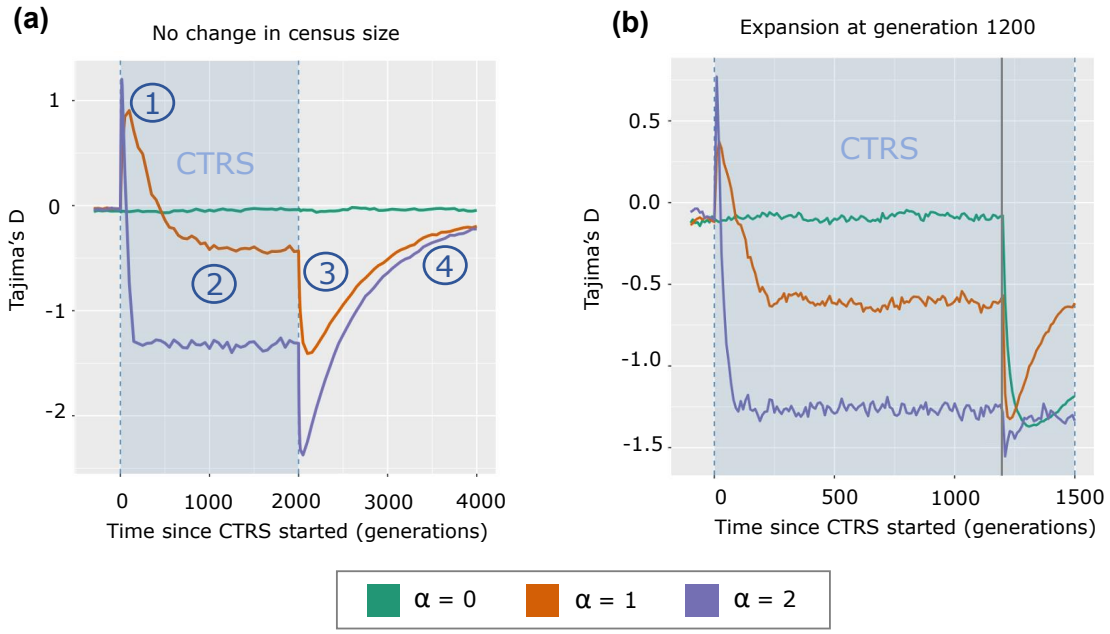

Figure 4: Tajima's D through time under various CTRS and demographic conditions. (a-b) The blue rectangle corresponds to the period when populations are under CTRS. Generations are counted from the beginning of CTRS. In all cases, the $b = 1$ model of variance in progeny size is used. (a) Tajima's D across generations for three values of α (0, 1, and 2), with a constant population size of 1000 individuals. (b) Tajima's D across generations for three values of α (0, 1, and 2). A fivefold expansion event occurs at generation 1200 (200 individuals to 1000 individuals — gray vertical line).

show that the 4-fold contraction indeed yields a higher number of polytomies than the neutral case, but a lower number of polytomies compared with the scenario of CTRS (Supp. Fig. S5a). Thus, the increased number of polytomies under CTRS is caused not only by the contraction of the effective size, but also by the transmission property of CTRS. The same comparison for I_b shows that none of the imbalance under CTRS is due to the contraction of effective size, as the mean imbalance after contraction is equal to the mean imbalance of the neutral case, with a higher variance due to the smaller population size (Supp. Fig. S5b).

The distribution of I_b across the genome was bell-shaped and unimodal for all tested strengths of CTRS ($\alpha = 0$, 1, and 2), with a shift toward high values when α increased (Supp. Fig. S6). This is because CTRS is not conveyed by any locus in particular, unlike natural selection, for which we could expect in some cases a multimodal distribution due to imbalanced trees in the region under selection and balanced trees elsewhere in the genome. Unlike the distribution of Tajima's D (Supp. Fig. S3), the distribution of I_b does not evolve during the process of CTRS, as shown when comparing the distributions after 20 and 500 generations of CTRS (Supp. Fig. S6). In fact, I_b is only impacted by the imbalance property of coalescent trees and thus only displays its effects, which are constant through time after the first few generations, contrary to Tajima's D, which is affected by imbalance and by changes in effective size as well, with the latter's effects depending strongly on time.

3.2.4 Short-lasting CTRS

We have thus far simulated cases of long-lasting CTRS, in order to investigate the values of the different statistics at the equilibrium state under CTRS (Figure 4). However, as the CTRS duration could be much shorter in reality, we also investigated cases where CTRS lasted for only a few generations. This situation was simulated for both low ($b = \infty$) and high variance in progeny-size ($b = 1$). We show that two or three generations of CTRS are sufficient to have an impact on genetic statistics (Supp. Fig. S7). Tajima's D displays an effect under medium ($\alpha = 1$) and high levels of CTRS ($\alpha = 2$), for both models of variance in progeny-size ($b = \infty$ and $b = 1$). Conversely, I_b seems affected under medium levels of CTRS only in the case of high variance in progeny size. Note that these realistic short periods of

CTRS lead to an increase in Tajima's D toward positive values due to the effective size contraction, as explained above. Finally, we show that after such a short period of CTRS, a few generations without CTRS are not sufficient to erase the effects on the genome (Supp. Fig. S7).

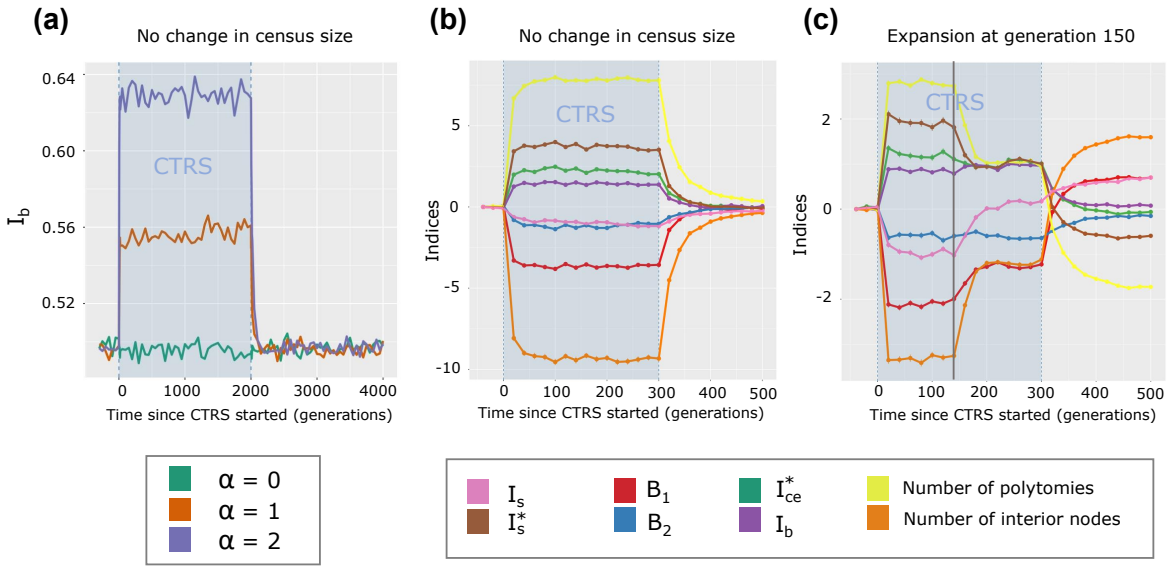

Figure 5: Imbalance indices over time. (a-c) The blue rectangle corresponds to the period when populations are under CTRS. Generations are counted from the beginning of CTRS. In all cases, the $b = 1$ model of variance in progeny size is used. (a) I_b across generations for three values of α (0, 1, and 2). (b) Various indices across generations for $\alpha = 1$. For each point, bars show the standard error of the mean. (c) Various indices across generations for $\alpha = 1$. An expansion event occurs at generation 150 (vertical gray line). For each point, bars show the standard error of the mean.

3.2.5 CTRS detection

Some indices seem to be more effective for CTRS detection than others (Figure 5b). When $\alpha = 1$, of all tree (im)balance indices, B_1 and I_s^* are the most affected, with a shift of 3 to 4 SD, while this shift is only between 1 and 2 SD for other (im)balance indices such as I_b, I_s, B_2. I_{ca}^* and I_{ce}^*, the two Colless indices handling polytomies, display a similar pattern with a shift of 2 SD (Supp. Fig. S8). However, I_{ce}^* seems slightly more affected by CTRS, due probably to its algorithm focusing on children with an extreme number of leaves (see Methods). The number of interior nodes and the number of polytomies are affected by CTRS more than all other measured indices, with a shift of 8 to 9 SD (Figure 5b). Interestingly, each of these indices seems to contain specific information about tree topology, as the correlations between their absolute values range between 0.99 and -0.17, although they all are correlated to α (Supp. Fig. S9). Thus, a method combining various indices (e.g., using approximate Bayesian computation) might be able to detect CTRS from population genomic data more accurately than a method using a single index. Furthermore, not all indices are robust to demographic events, as shown in Figure 5c: only I_b and B_2 seem unchanged when an expansion occurs during CTRS (vertical gray line at generation 150), with a small change for I_{ce}^* and wider changes for other indices. The remaining indices are all affected by the demographic event, although they still show tree imbalance of samples collected after the event (except for I_s, which reaches 0 soon after the event).

As with many evolutionary processes, the ability to detect CTRS also depends on the number of sampled individuals and loci. We assessed the effect of these two parameters on our ability to discriminate two scenarios using a Wilcoxon rank test: one of 20 generations of CTRS (strength $\alpha = 1$) before present and one without CTRS ($\alpha = 0$). We show that for all four studied summary statistics (i.e., I_b, B_2, Number of polytomies and Tajima's D), power increases with both the number

of sampled individuals and the number of sampled loci (Supp. Fig. S10). The number of polytomies and Tajima's D are the most effective indices, with the first index reaching a power above 0.95 (at Type I error = 0.01) for 60 genomic regions of 1 Mb and 10 sampled individuals, and the second reaching this power for 100 genomic regions of 1 Mb and 10 sampled individuals. However, as shown previously, both indices are also impacted by changes in census population size and cannot thus be used alone for CTRS inference. Conversely, I_b and B_2 are independent from changes in population size, but display a much lower power of detection compared with the two previous indices. I_b needs 30 individuals and 100 genomic regions of 1 Mb in order to reach a power of 0.95, while B_2 needs 90 individuals and 100 genomic regions of 1 Mb to reach this power of detection. For CTRS detection, the number of individuals seems to have a stronger impact on power of detection than the number of genomic regions, with a power above 0.9 reached with I_b for 100 individuals and 10 independent regions of 1 Mb, compared with a power of 0.15 with 10 individuals and 100 independent regions of 1 Mb, possibly due to the need to have a minimum number of sampled individuals in order to assess topological properties of the population coalescent trees. As stated above, we expect a combination of multiple indices using methods such as ABC to be even more effective for CTRS estimation from genomic data, compared with single indices. Additionally, using the distribution of indices along the genome might provide more information about past CTRS compared with the use of mere averages.

In conclusion, the evolution of Tajima's D and imbalance measures over time highlights the complexity and the timing of CTRS impacts on population genetics. When CTRS starts or stops, sudden changes in effective population size occur. During the process, CTRS affects coalescent tree topology (imbalance and number of polytomies) and branch lengths with a nonhomogenous reduction (young branches less impacted than old branches). Imbalance is due to the transmission process, which yields asymmetrical genealogies. The higher number of polytomies stems from the higher coalescence rate. The nonhomogenous branch length reduction is similar to what occurs during an expansion. Although the effective population size remains stable during CTRS, a pseudoexpansion occurs, due to the expansion of large family lineages, which is compensated by the extinction of small family lineages (Sibert *et al.*, 2002). All of these mechanisms affect the genomic signal commonly used for population genetic inferences, and the next section will illustrate, based on simulations of an instantaneous expansion, how demographic inference is impacted both before and after CTRS equilibrium.

3.3 Impact of CTRS on demographic inference

In this section, we investigate the impact of CTRS on demographic inference before and after CTRS equilibrium. In the first case, the genomic signal of expansion is affected by the distortion in tree topology (i.e., imbalance and higher number of polytomies) and by the recent change in effective population size, while in the second case only changes in tree topology remain. We explored the "Before CTRS equilibrium" scenario by inferring demography 20 generations after the beginning of CTRS, and the "At equilibrium" scenario by inferring demography 1500 generations after the beginning of CTRS. The 5-fold expansion event to be inferred occurs in both scenarios 300 generations before the inference (more details in Methods).

Before CTRS equilibrium, we measured a strong bias in the demography inferred by $\delta a \delta i$. When $\alpha = 1$, the inferred growth factor has a median of 3 instead of 5 (relative bias = -0.37, MSRE = 0.18, compared with 0 and 0.04, respectively, for $\alpha = 0$) (Figure 6c). $\delta a \delta i$ inferences are based solely on the SFS. After 20 generations of CTRS and without any change in census population size, SFS shows a marked deficit of rare alleles due to the contraction of effective population size caused by the initiation of CTRS, and an excess of common alleles due to this contraction combined with the presence of many related individuals coming from large family lineages (Figure 6a). Conversely, in a scenario of 20 generations of CTRS following an event of expansion, the SFS for $\alpha = 1$ is expectedly a mix between the expansion-only pattern ($\alpha = 0$) and the CTRS pattern for $\alpha = 1$ (Figure 6b). In this case, the SFS displays a smaller excess of rare alleles compared with the expansion-only pattern. Since the excess of rare alleles is the main signal of expansions, a smaller expansion is inferred. The contraction of the effective population size due to the initiation of CTRS reduces the excess of rare alleles caused by the expansion event, yielding an inference of a smaller growth factor. Time since the demographic event is also inferred less accurately after a period of 20 generations of CTRS (for $\alpha = 0$: relative bias = -0.17, MSRE = 0.06; for $\alpha = 1$: relative bias = 0.22, MSRE = 0.21).

At CTRS equilibrium, for $\alpha = 1$, a median growth factor of 3.8 is inferred instead of 5 (relative bias = -0.18, MSRE = 0.16, compared with -0.01 and 0.04, respectively, for $\alpha = 0$) (Figure 6g). The

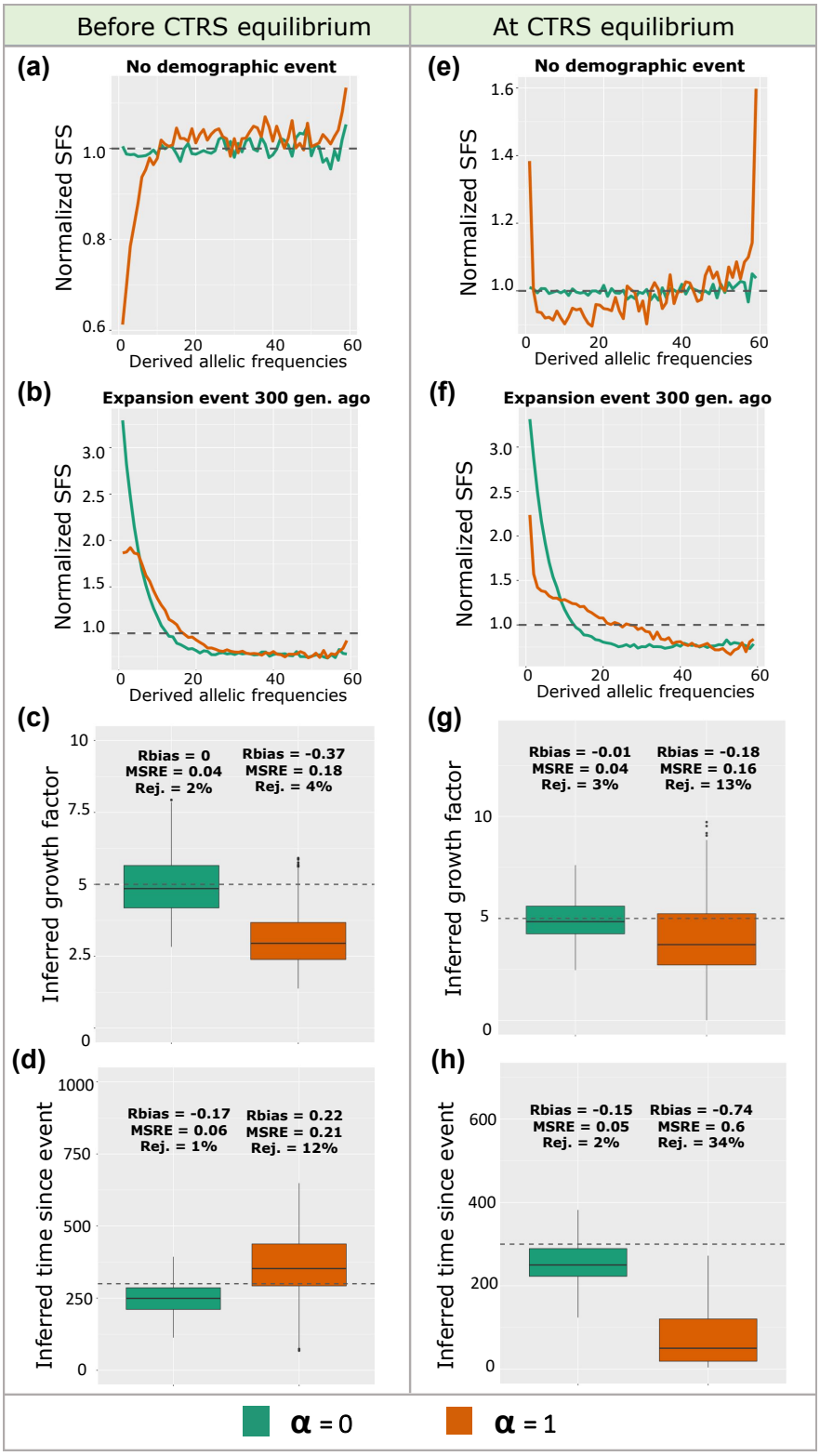

Figure 6: SFS and $\delta a \delta i$ inference of expansion parameters at two stages of CTRS. (a) and (e) SFS for $\alpha = 0$ and 1 with no demographic event. (b) and (f) SFS for $\alpha = 0$ and 1 after a 5-fold expansion 300 generations ago. (c) and (g) inferred growth factor for $\alpha = 0$ and 1, after a 5-fold expansion 300 generations ago. (d) and (h) inferred number of generations since expansion for $\alpha = 0$ and 1, after a 5-fold expansion 300 generations ago. (a-d) Scenario "Before CTRS equilibrium" (20 generations of CTRS before present). (e-f) Scenario "At CTRS equilibrium" (1500 generations of CTRS before present). MSRE, relative bias and percentage of rejected replicates displayed above each boxplot. In all cases, the $b = 1$ model of variance in progeny size is used.

SFS at CTRS equilibrium with no demographic event is U-shaped (Figure 6e). Tree imbalance and the higher number yield the excess of rare and common alleles, while nonhomogenous reduction of branch lengths contributes to the excess of rare alleles. When a demographic expansion occurs at CTRS equilibrium, the SFS displays a tilted U-shape, with less excess of rare alleles in comparison to the expansion-only scenario (Figure 6f). This is due to the smaller effective population size during the generations where CTRS occurs, which induces an accelerated loss of part of the rare alleles created by the fivefold expansion event. Since rare alleles are the main traces of this past expansion event, a smaller expansion is inferred. The inferred time since the demographic event when the population experienced 1500 generations of CTRS was strongly biased, with a median inference of 50 generations since the demographic event instead of 300 ($\alpha = 0$: relative bias = -0.15, MSRE = 0.05; $\alpha = 1$: relative bias = -0.74, MSRE = 0.6) (Figure 6h).

We thus showed that after a period of CTRS, whether short (20 generations) or long (1500 generations), past growth factors of expansion events are underestimated with an SFS-based inference method, due to a lack of rare alleles compared with the neutral case scenario. The time since the expansion event can be largely underestimated if it happened after a long period of CTRS and slightly overestimated after a short period of CTRS.

4 Conclusions

Many studies evaluating CTRS strength in human populations rely on the computation of correlations between parents and children progeny size from pedigree datasets (Murphy, 1999). However, we show here that this measure cannot by itself account for the magnitude of CTRS effects on population genetics. Indeed, under the high variance in progeny size model ($b = 1$), correlations are lower than under the low variance model ($b = \infty$), while the impacts on population genetics are increased. Thus, a more precise evaluation of CTRS from pedigree data would require considering the distributions of parents and child progeny sizes in addition to the correlation values. Furthermore, the higher correlations under the low variance model ($b = \infty$) could explain the higher correlations observed in populations that exhibited a demographic transition (Murphy, 1999; Jennings *et al.*, 2012; Jennings and Leslie, 2013). Indeed, a main characteristic of this transition is a decrease in progeny size variance. Finally, we observe that CTRS has a stronger impact on effective size than the variance introduced in the model. This result is supported by measurements in the Saguenay–Lac-Saint-Jean population for similar levels of progeny size correlation (Heyer *et al.*, 2012).

CTRS impacts genomic diversity in two ways: (i) when CTRS begins or ends, populations undergo a decrease (resp. increase) in effective size that impacts several population genetic statistics such as Tajima's D and SFS. This lower effective size stems from the increased variance in progeny size under CTRS and from the transmission component itself. We could show that the latter accounts for most part of the decrease in effective population size under CTRS. (ii) During the CTRS process and shortly after the process stops, coalescent tree topologies (i.e., tree shape properties that are not related to branch length) are distorted, which also impacts Tajima's D and SFS. When CTRS lasts long enough, the effect of the change in effective size disappears while tree topology distortion persists, inducing lower genetic diversity and a U-shaped SFS. These two processes start together but have different dynamics, yielding a complex effect on population genetics over time.

We showed that the distortion in coalescent tree topology affects two topological properties: (1) trees are more imbalanced, which can be shown with balance and imbalance indices, and (2) the number of polytomies increases. In theory, both of these effects could happen independently, as binary trees can be imbalanced and polytomies do not necessarily induce imbalance. However, under CTRS, we show that trees undergo a complex change in their topology, with an interplay between these two properties of imbalance and polytomies. These two effects increase the proportions of rare and common alleles, while a nonhomogenous reduction in branch lengths (Sibert *et al.*, 2002) increases only the proportion of rare alleles, yielding a U-shaped SFS. Further studies could evaluate the relative impacts and possible interactions between these processes.

The impact of CTRS on SFS explains why the SFS-based demographic inference performed by $\delta a \delta i$ was biased for populations undergoing CTRS. After a few generations of CTRS, the growth factors of past expansion events are underestimated. This result implies that past expansions, such as the Neolithic ones, might be underestimated in populations experiencing CTRS, at least when inferred based on SFS. After many generations under CTRS, the timing of expansion is strongly underestimated

as well. Furthermore, due to the decrease in effective population size induced by CTRS, past expansion signals were lost more rapidly, when compared with scenarios without CTRS. Similarly, the signal of other past events, such as bottlenecks, selection or migration, is expected to be erased more rapidly in the presence of CTRS. We established that CTRS impacts an SFS-based inference method and expect other approaches to be affected given that CTRS distorts coalescent trees, which are directly or indirectly at the core of any inference method. CTRS is thus one more process among others that can affect demographic inference (e.g., purifying and background selection (Johri *et al.*, 2021; Pouyet *et al.*, 2018), biased gene conversion (Pouyet *et al.*, 2018), population structure (Mazet *et al.*, 2016), selection, gene conversion, and biased sampling in microbial populations (Lapierre *et al.*, 2016)).

To disentangle the effects of demographic events from CTRS, imbalance indices that are unaffected by variations in the census population size can be used. We showed that the power of detection of CTRS from genomic data is less impacted by the number of independent regions than by the number of sequenced individuals that should be high enough, a condition easily achieved with modern datasets. However, these indices are computed from coalescent trees which first need to be reconstructed from genomic data (e.g., using tools such as ARGweaver (Rasmussen *et al.*, 2014), tsinfer (Kelleher *et al.*, 2019), or relate (Speidel *et al.*, 2019)). This tree reconstruction step might not be able to infer a perfectly accurate topology, yielding potential biases in the estimated (im)balance indices. Moreover, in addition to the expected imprecision of the reconstruction of neutral trees, the behavior of these tools under CTRS remains to be checked. Another possibility would be to build and train deep learning networks directly on raw genomic data without reconstructing coalescent trees, as in Sanchez *et al.* (2021), which would prevent the introduction of biases due to tree reconstruction, but might require a larger amount of simulated data for training. To generate this large dataset, it would be useful to develop a backward coalescent model of CTRS, as forward-in-time simulations are particularly time-consuming.

Finally, we should address the question of the similarity between CTRS and natural selection: in both cases, some individuals have more offspring than others and transmit this higher fertility to their descendants. However, in the case of CTRS, fertility is culturally transmitted, whereas for selection, it is genetically transmitted. The question is to what extent these processes affect the genome differently. Without recombination, one might expect qualitatively similar effects of the two processes on the genome: lower diversity and similar patterns for Tajima's D over time. Moreover, tree topology is also expected to be distorted with an increase in imbalance (Fay and Wu, 2000; Li, 2011; Li and Wiehe, 2013) and number of polytomies (Durrett and Schweinsberg, 2005; Neher and Hallatschek, 2013) under selection. The resemblance of the two processes is confirmed by a similar U-shaped signature in SFS: selection also yields an excess of rare (Braverman *et al.*, 1995) and common alleles (Fay and Wu, 2000).

However, a fairly clear difference exists between the CTRS model (based on the α parameter) used here and the commonly used model of positive selection (based on the selection coefficient s, (Wright, 1932)). Under this model of selection, the beneficial allele can go to fixation, and selection stops at that point. However, in the case of CTRS, the model is constructed in such a way that the TRS may continue indefinitely. The CTRS model would more closely resemble a positive selection model with a high mutation rate, preventing fixation. This difference between the two models makes sense relative to reality: cultural transmission can be expected to be quite inaccurate in real life compared with genetic transmission. This argument of "high mutation rate" in cultural transmission has been used to resolve the so-called Fisher's paradox (Pettay *et al.*, 2005): how can correlations between parents' and children's progeny size remain positive over time given the expected erosion of variance in the fertility phenotype? The answer would be that these correlations stem from a CTRS and not a genetic TRS. Thus, the unfaithful cultural transmission of fertility would explain why variance is maintained, with the "high mutation rate" preventing the "fixation" of high-fertility cultural traits (Heyer *et al.*, 2012). This difference in fixation between the two models might yield distinctive dynamics in population genetics statistics. To further compare CTRS and selection models, an analytical reconciliation that would link α to the selection coefficient would be pertinent.

A second difference between CTRS and selection appears when recombination is considered. In this case, the selection signal is restricted over time to the locus under selection, as recombination events accumulate, with a remaining local effect on nearby loci due to hitchhiking (Smith and Haigh, 1974). The length of the region impacted by hitchhiking depends on the recombination rate, as well as on the time under which selection has been acting. When fixation occurs, this time is equivalent to the time to

fixation, which is inversely proportional to the selection coefficient s (Kim and Stephan, 2002; Stephan, 2019). In human populations, even selection events that started rather recently have been shown to give rise to a signal restricted to only a few megabases. For example, in the case of the selection for lactase persistence in Africa (event dated to ∼7000 years ago), the selection signal decreases very rapidly over the 3 Mb sequenced (Tishkoff *et al.*, 2007). An even more recent selection event, such as the one on the 3p12.1 chromosomal region in Mongolians, associated with energy metabolism and reproductive traits, dated to approximately 50 generations ago (∼1500 years), is almost undetectable outside the 4 Mb region around the locus under selection (Nakayama *et al.*, 2017). Conversely, in the case of CTRS, the effects are uniform over the whole genome since the transmission of fertility is not conveyed by genetics: we showed in this paper the shift of the whole distribution of tree imbalances in the genome toward higher values. We expect the distribution of indices across the genome to be quite different in the case of selection, which would help distinguish between the two processes.

We can go farther and compare polygenic selection to CTRS, because of their propensity to affect simultaneously distant loci in the genome. In particular, background selection, which has this ability to affect large parts of the genome (Pouyet *et al.*, 2018), could strongly resemble CTRS in its effects. Because of their potential similarity, distinguishing highly polygenic selection from CTRS might be troublesome. However, it seems unlikely that even highly polygenic selection would have an effect identical to CTRS for several reasons. First, the neutral parts of the genome are under the effect of CTRS but not under that of polygenic selection (e.g., Pouyet *et al.* (2018) identified a set of SNPs that are mostly unaffected by background selection). Second, in a polygenic selection, selective pressure may have different parameters depending on the gene: the temporality may differ (selective pressure does not start at the same time on each gene) as well as intensity (different selection coefficients for each gene), yielding different coalescent trees across the genome (each gene tree telling its own history). In fact, theoretical analyses showed different temporal dynamics in polygenic adaptation, with large effect alleles contributing first, followed by small/intermediate-effect alleles (Hayward and Sella, 2022; Barghi *et al.*, 2020). This process has been shown to be responsible for maize domestication, with a central transcription factor (*teosinte branched 1*) driving adaptation (Studer *et al.*, 2011), although most of the network controlled by this gene displays a selection signal as well (Wang *et al.*, 1999; Studer *et al.*, 2017; Barghi *et al.*, 2020). Conversely, CTRS will tend to create trees that look similar across the genome, since they are all affected uniformly by the same cultural history (a single α parameter for the whole genome). Third, populations exchanging migrants will tend to have the same alleles selected by multigenetic selection, whereas nongenetic TRS will select for different alleles in each population (alleles randomly carried by large family lineages). Fourth, under polygenic selection, genes can undergo a complex effect, combining not only the effects of their selection pressure, but also the effects of nearby genes due to hitchhiking (Barton, 1995). This competing effect would not happen under CTRS only, adding another difference between the effects of CTRS and of highly polygenic selection. Ultimately, these three listed differences might help distinguish the two processes in real data.

Furthermore, one may ask what happens when CTRS and selection are combined, which might be the case in a number of populations. Competition between selection and CTRS might arise in the case of a culturally fertile lineage carrying a disadvantageous allele. In fact, Austerlitz and Heyer (1998) have shown that CTRS can increase the propensity of a population to maintain genetic diseases. This increase in genetics disease can also stem from the reduction in diversity created by CTRS, under which conditions, selection is less effective. Studying coalescent tree shapes under the combined effects of selection and CTRS is also interesting: will trees be even more imbalanced compared with CTRS alone, or is imbalance already saturated by CTRS? It is also possible that the sum of the two processes will result in more balanced trees due to the aforementioned competition between them. The study of the combination of these two processes is crucial to be able to distinguish them in real populations, where both are likely to happen, in order to find their respective impact on genetic diversity and tree topologies.

Finally, the analysis of CTRS provided here might be valid for any TRS that is not genetic. For example, ecological inheritance (Odling-Smee, 1988; Danchin *et al.*, 2011), where an individual passes on its environment to its offspring, could yield a similar process provided that: (1) the population is settled in diverse environments, (2) the fitness varies with the environment, and (3) there is a vertical transmission of the environment (Bonduriansky and Day, 2018). These conditions might be achieved in plants whose seeds disperse little (Danchin *et al.*, 2011). Therefore, although the literature has

focused on *cultural TRS* until now (Blum *et al.*, 2006; Heyer *et al.*, 2012, 2015), one could generalize this evolutionary process and call it *nongenetic TRS*.

5 Data availability

The SLiM code used to generate the simulated data and the Python code for summary statistics computing and $\delta a \delta i$ inference can be found at https://github.com/jeremyguez/CTRS.

6 Acknowledgments

We thank the editor and three anonymous reviewers for their helpful comments and suggestions. We thank Matteo Fumagalli, Olivier François, Aurélien Tellier, Fanny Pouyet, Jean-Tristan Brandenburg, Théophile Sanchez, Romain Laurent, Ferdinand Petit and Arnaud Quelin for the insightful interactions.

7 Funding

JG was supported by a French National Center for Scientific Research (CNRS) fellowship: 80Prime (TransIA). FB was supported by Dr. Max Rössler, the Walter Haefner Foundation and the ETH Zürich Foundation. JC was supported by the Human Frontier Science Project (number RGY0075/2019). We also thank ANR-20-CE45-0010-01 RoDAPoG.

8 Conflicts of interest

The authors declare that there is no conflict of interest.

References

Austerlitz F, Heyer E. 1998. Social transmission of reproductive behavior increases frequency of inherited disorders in a young-expanding population. Proceedings of the National Academy of Sciences. 95:15140–15144.

Barber JS. 2001. The intergenerational transmission of age at first birth among married and unmarried men and women. Social Science Research. 30:219–247.

Barghi N, Hermisson J, Schlötterer C. 2020. Polygenic adaptation: a unifying framework to understand positive selection. Nature Reviews Genetics. 21:769–781. Number: 12 Publisher: Nature Publishing Group.

Barton NH. 1995. Linkage and the limits to natural selection. Genetics. 140:821–841.

Beichman AC, Huerta-Sanchez E, Lohmueller KE. 2018. Using genomic data to infer historic population dynamics of nonmodel organisms. Annual Review of Ecology, Evolution, and Systematics. 49:433–456.

Bersaglieri T, Sabeti PC, Patterson N, Vanderploeg T, Schaffner SF, Drake JA, Rhodes M, Reich DE, Hirschhorn JN. 2004. Genetic signatures of strong recent positive selection at the lactase gene. The American Journal of Human Genetics. 74:1111–1120.

Bienvenu F, Cardona G, Scornavacca C. 2021. Revisiting Shao and Sokal's B_2 index of phylogenetic balance. Journal of Mathematical Biology. 83:1–43.

Blum MGB, Heyer E, François O, Austerlitz F. 2006. Matrilineal fertility inheritance detected in hunter–gatherer populations using the imbalance of gene genealogies. PLOS Genetics. 2:e122.

Boitard S, Rodríguez W, Jay F, Mona S, Austerlitz F. 2016. Inferring population size history from large samples of genome-wide molecular data - an approximate Bayesian computation approach. PLOS Genetics. 12:1–36.

Bonduriansky R, Day T. 2018. *Extended Heredity: A New Understanding of Inheritance and Evolution*. Princeton University Press. Princeton (New Jersey). Google-Books-ID: 1j63DwAAQBAJ.

Brandenburg JT, Austerlitz F, Toupance B. 2012. Impact of fertility transmission and other sociodemographic factors on reproductive success and coalescent trees. Genetics Research. 94:121–131.

Braverman JM, Hudson RR, Kaplan NL, Langley CH, Stephan W. 1995. The hitchhiking effect on the site frequency spectrum of DNA polymorphisms. Genetics. 140:783–796.

Chaix R, Austerlitz F, Khegay T, Jacquesson S, Hammer MF, Heyer E, Quintana-Murci L. 2004. The genetic or mythical ancestry of descent groups: Lessons from the y chromosome. The American Journal of Human Genetics. 75:1113–1116.

Colless DH. 1982. Review of "Phylogenetics: the theory and practice of phylogenetic systematics". Systematic Zoology. 31:100–104.

Danchin E, Charmantier A, Champagne FA, Mesoudi A, Pujol B, Blanchet S. 2011. Beyond DNA: integrating inclusive inheritance into an extended theory of evolution. Nature Reviews Genetics. 12:475–486. Number: 7 Publisher: Nature Publishing Group.

de Valk HA. 2013. Intergenerational discrepancies in fertility preferences among immigrant and Dutch families. The History of the Family. 18:209–225.

Duncan OD, Freedman R, Coble JM, Slesinger DP. 1965. Marital fertility and size of family of orientation. Demography. 2:508–515.

Durrett R, Schweinsberg J. 2005. A coalescent model for the effect of advantageous mutations on the genealogy of a population. Stochastic Processes and their Applications. 115:1628–1657.

Engh AL, Esch K, Smale L, Holekamp KE. 2000. Mechanisms of maternal rank 'inheritance' in the spotted hyaena, *Crocuta crocuta*. Animal Behaviour. 60:323–332.

Ewens WJ. 2016. Effective population size, In: Kliman RM, editor, *Encyclopedia of evolutionary biology*, Academic Press. Waltham (MA). pp. 494–497.

Excoffier L, Dupanloup I, Huerta-Sánchez E, Sousa VC, Foll M. 2013. Robust demographic inference from genomic and SNP data. PLOS Genetics. 9:e1003905.

Fay JC, Wu CI. 2000. Hitchhiking under positive Darwinian selection. Genetics. 155:1405–1413.

Frere CH, Krutzen M, Mann J, Connor RC, Bejder L, Sherwin WB. 2010. Social and genetic interactions drive fitness variation in a free-living dolphin population. Proceedings of the National Academy of Sciences. 107:19949–19954.

Gagnon A, Heyer E. 2001. Intergenerational correlation of effective family size in early Québec (Canada): Correlation of effective family size. American Journal of Human Biology. 13:645–659.

Gagnon A, Toupance B, Tremblay M, Beise J, Heyer E. 2006. Transmission of migration propensity increases genetic divergence between populations. American Journal of Physical Anthropology. 129:630–636.

Gerbault P, Liebert A, Itan Y, Powell A, Currat M, Burger J, Swallow DM, Thomas MG. 2011. Evolution of lactase persistence: an example of human niche construction. Philosophical Transactions of the Royal Society B: Biological Sciences. 366:863–877.

Gutenkunst RN, Hernandez RD, Williamson SH, Bustamante CD. 2009. Inferring the joint demographic history of multiple populations from multidimensional SNP frequency data. PLOS Genetics. 5:e1000695.

Haller BC, Messer PW. 2019. SLiM 3: Forward genetic simulations beyond the Wright–Fisher model. Molecular Biology and Evolution. 36:632–637.

Hayward LK, Sella G. 2022. Polygenic adaptation after a sudden change in environment. eLife. 11:e66697.

Heyer E, Brandenburg JT, Leonardi M, Toupance B, Balaresque P, Hegay T, Aldashev A, Austerlitz F. 2015. Patrilineal populations show more male transmission of reproductive success than cognatic populations in Central Asia, which reduces their genetic diversity: Cultural transmission of fitness. American Journal of Physical Anthropology. 157:537–543.

Heyer E, Chaix R, Pavard S, Austerlitz F. 2012. Sex-specific demographic behaviours that shape human genomic variation: sex-specific behaviours and genomic variation. Molecular Ecology. 21:597–612.

Jay F, Boitard S, Austerlitz F. 2019. An ABC method for whole-genome sequence data: Inferring paleolithic and neolithic human expansions. Molecular Biology and Evolution. 36:1565–1579.

Jennings J, Leslie P. 2013. Differences in intergenerational fertility associations by sex and race in Saba, Dutch Caribbean, 1876-2004. The history of the family : an international quarterly. 18:135–153.

Jennings J, Sullivan A, Hacker J. 2012. Intergenerational Transmission of Reproductive Behavior during the Demographic Transition. The Journal of interdisciplinary history. 42:543–69.

Johri P, Riall K, Becher H, Excoffier L, Charlesworth B, Jensen JD. 2021. The impact of purifying and background selection on the inference of population history: Problems and prospects. Molecular Biology and Evolution. 38:2986–3003.

Kawai M. 1958. On the rank system in a natural group of Japanese monkey (I): the basic and dependent rank. Primates. 1:111–130.

Kelleher J, Etheridge AM, McVean G. 2016. Efficient Coalescent Simulation and Genealogical Analysis for Large Sample Sizes. PLOS Computational Biology. 12:e1004842. Publisher: Public Library of Science.

Kelleher J, Wong Y, Wohns AW, Fadil C, Albers PK, McVean G. 2019. Inferring whole-genome histories in large population datasets. Nature Genetics. 51:1330–1338.

Kelly MJ. 2001. Lineage loss in serengeti cheetahs: Consequences of high reproductive variance and heritability of fitness on effective population size. Conservation Biology. 15:11.

Kim Y, Stephan W. 2002. Detecting a Local Signature of Genetic Hitchhiking Along a Recombining Chromosome. Genetics. 160:765–777.

Kingman JFC. 1982. The coalescent. Stochastic Processes and their Applications. 13:235–248.

Kohler HP, Rodgers JL, Christensen K. 1999. Is fertility behavior in our genes? Findings from a Danish twin study. Population and Development Review. 25:253–288.

Kolk M. 2014. Multigenerational transmission of family size in contemporary Sweden. Population Studies. 68:111–129.

Lapierre M, Blin C, Lambert A, Achaz G, Rocha EPC. 2016. The impact of selection, gene conversion, and biased sampling on the assessment of microbial demography. Molecular Biology and Evolution. 33:1711–1725.

Lapierre M, Lambert A, Achaz G. 2017. Accuracy of demographic inferences from the Site Frequency Spectrum: The case of the Yoruba population. Genetics. 206:439–449.

Lawson DW, Mace R. 2011. Parental investment and the optimization of human family size. Philosophical Transactions of the Royal Society B: Biological Sciences. 366:333–343.

Li H. 2011. A New Test for Detecting Recent Positive Selection that is Free from the Confounding Impacts of Demography. Molecular Biology and Evolution. 28:365–375.

Li H, Wiehe T. 2013. Coalescent Tree Imbalance and a Simple Test for Selective Sweeps Based on Microsatellite Variation. PLOS Computational Biology. 9:e1003060. Publisher: Public Library of Science.

Liu X, Fu YX. 2020. Stairway Plot 2: demographic history inference with folded SNP frequency spectra. Genome Biology. 21:280.

Mazet O, Rodríguez W, Grusea S, Boitard S, Chikhi L. 2016. On the importance of being structured: instantaneous coalescence rates and human evolution—lessons for ancestral population size inference? Heredity. 116:362–371.

Mills MC, Tropf FC. 2015. The biodemography of fertility: A review and future research frontiers. KZfSS Kölner Zeitschrift für Soziologie und Sozialpsychologie. 67:397–424.

Mondal M, Bertranpetit J, Lao O. 2019. Approximate Bayesian computation with deep learning supports a third archaic introgression in Asia and Oceania. Nature Communications. 10:246.

Mulder MB, Bowles S, Hertz T, Bell A, Beise J, Clark G, Fazzio I, Gurven M, Hill K, Hooper PL *et al.* 2009. Intergenerational wealth transmission and the dynamics of inequality in small-scale societies. Science. 326:682–688.

Murphy M. 1999. Is the relationship between fertility of parents and children really weak? Biodemography and Social Biology. 46:122–145.

Murphy M. 2013. The intergenerational transmission of reproductive behaviour: comparative perspectives. The History of the Family. 18:107–115.

Murphy M, Wang D. 2001. Family-level continuities in childbearing in low-fertility societies. European Journal of Population / Revue Européenne de Démographie. 17:75–96.

Nakayama K, Ohashi J, Watanabe K, Munkhtulga L, Iwamoto S. 2017. Evidence for Very Recent Positive Selection in Mongolians. Molecular Biology and Evolution. 34:1936–1946.

Neher RA, Hallatschek O. 2013. Genealogies of rapidly adapting populations. Proceedings of the National Academy of Sciences. 110:437–442.

Odling-Smee FJ. 1988. Niche-constructing phenotypes, In: , The MIT Press. Cambridge, MA, US. pp. 73–132.

Pettay JE, Kruuk LEB, Jokela J, Lummaa V. 2005. Heritability and genetic constraints of life-history trait evolution in preindustrial humans. Proceedings of the National Academy of Sciences. 102:2838–2843.

Pluzhnikov A, Nolan DK, Tan Z, McPeek MS, Ober C. 2007. Correlation of Intergenerational Family Sizes Suggests a Genetic Component of Reproductive Fitness. The American Journal of Human Genetics. 81:165–169. Publisher: Elsevier.

Potter RG, Kantner JF. 1955. Social and psychological factors affecting fertility. XXVIII. The influence of siblings and friends on fertility. The Milbank Memorial Fund Quarterly. 33:246.

Pouyet F, Aeschbacher S, Thiéry A, Excoffier L. 2018. Background selection and biased gene conversion affect more than 95% of the human genome and bias demographic inferences. eLife. 7:e36317.

Rasmussen MD, Hubisz MJ, Gronau I, Siepel A. 2014. Genome-wide inference of ancestral recombination graphs. PLOS Genetics. 10:e1004342.

Rodgers JL, Kohler HP, Kyvik KO, Christensen K. 2001. Behavior genetic modeling of human fertility: findings from a contemporary Danish twin study. Demography. 38:14.

Sackin MJ. 1972. "Good" and "bad" phenograms. Systematic Biology. 21:225–226.

Sanchez T, Cury J, Charpiat G, Jay F. 2021. Deep learning for population size history inference: Design, comparison and combination with approximate Bayesian computation. Molecular Ecology Resources. 21:2645–2660.

Segurel L, Guarino-Vignon P, Marchi N, Lafosse S, Laurent R, Bon C, Fabre A, Hegay T, Heyer E. 2020. Why and when was lactase persistence selected for? Insights from Central Asian herders and ancient DNA. PLoS biology. 18:e3000742.

Shao KT, Sokal RR. 1990. Tree balance. Systematic Zoology. 39:266–276.

Sheehan S, Song YS. 2016. Deep learning for population genetic inference. PLOS Computational Biology. 12:1–28.

Sibert A, Austerlitz F, Heyer E. 2002. Wright–Fisher revisited: The case of fertility correlation. Theoretical Population Biology. 62:181–197.

Smith JM, Haigh J. 1974. The hitch-hiking effect of a favourable gene. Genetical Research. 23:23–35.

Sorokowski P, Sorokowska A, Danel DP. 2013. Why pigs are important in Papua? Wealth, height and reproductive success among the Yali tribe of West Papua. Economics & Human Biology. 11:382–390.

Speidel L, Forest M, Shi S, Myers SR. 2019. A method for genome-wide genealogy estimation for thousands of samples. Nature Genetics. 51:1321–1329.

Stephan W. 2019. Selective Sweeps. Genetics. 211:5–13.

Studer A, Zhao Q, Ross-Ibarra J, Doebley J. 2011. Identification of a functional transposon insertion in the maize domestication gene tb1. Nature Genetics. 43:1160–1163.

Studer AJ, Wang H, Doebley JF. 2017. Selection During Maize Domestication Targeted a Gene Network Controlling Plant and Inflorescence Architecture. Genetics. 207:755–765.

Swallow DM. 2003. Genetics of lactase persistence and lactose intolerance. Annual Review of Genetics. 37:197–219.

Terhorst J, Kamm JA, Song YS. 2017. Robust and scalable inference of population history from hundreds of unphased whole-genomes. Nature genetics. 49:303–309.

Tishkoff SA, Reed FA, Ranciaro A, Voight BF, Babbitt CC, Silverman JS, Powell K, Mortensen HM, Hirbo JB, Osman M *et al*. 2007. Convergent adaptation of human lactase persistence in Africa and Europe. Nature Genetics. 39:31–40. Number: 1 Publisher: Nature Publishing Group.

Wang RL, Stec A, Hey J, Lukens L, Doebley J. 1999. The limits of selection during maize domestication. Nature. 398:236–239.

Whitehead H. 1998. Cultural selection and genetic diversity in matrilineal whales. Science. 282:1708–1711.

Wright S. 1932. The Roles of Mutation, Inbreeding, crossbreeding and Selection in Evolution. In: . The Hague, The Netherlands. Pergamon Press.

Wright S. 1938. Size of population and breeding structure in relation to evolution. Science. 87:430–431.

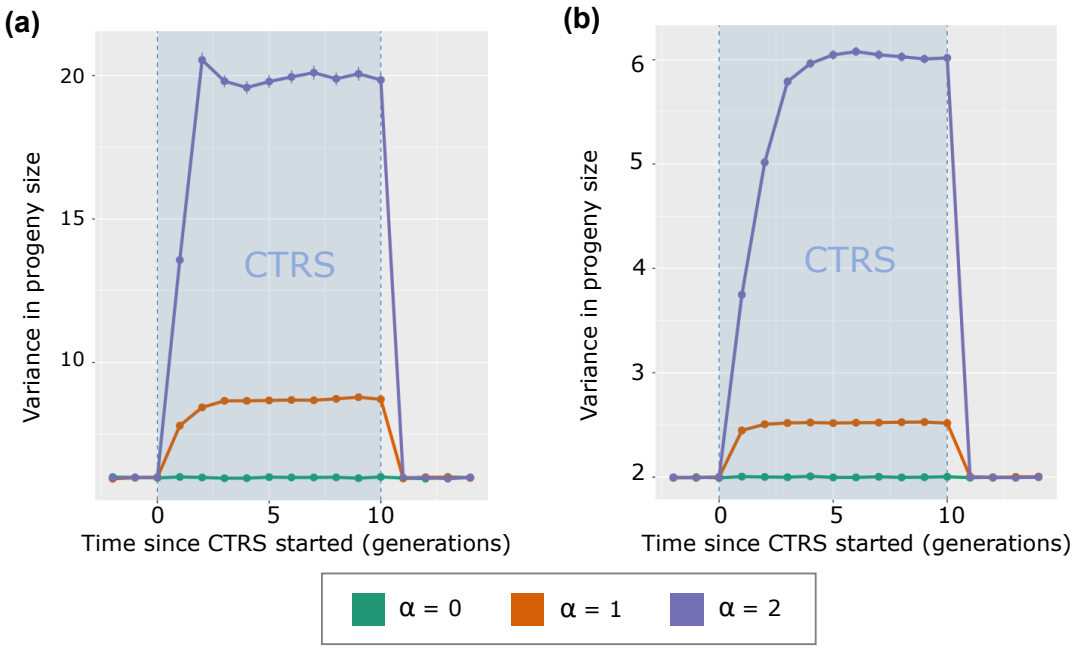

Figure S1: Variance of progeny size as a function of time for $\alpha = 0$, 1, and 2. The blue rectangle corresponds to the period when populations are under CTRS. Generations are counted from the beginning of CTRS. (a) $b = \infty$ model (low variance of progeny size). (b) $b = 1$ model (high variance of progeny size).

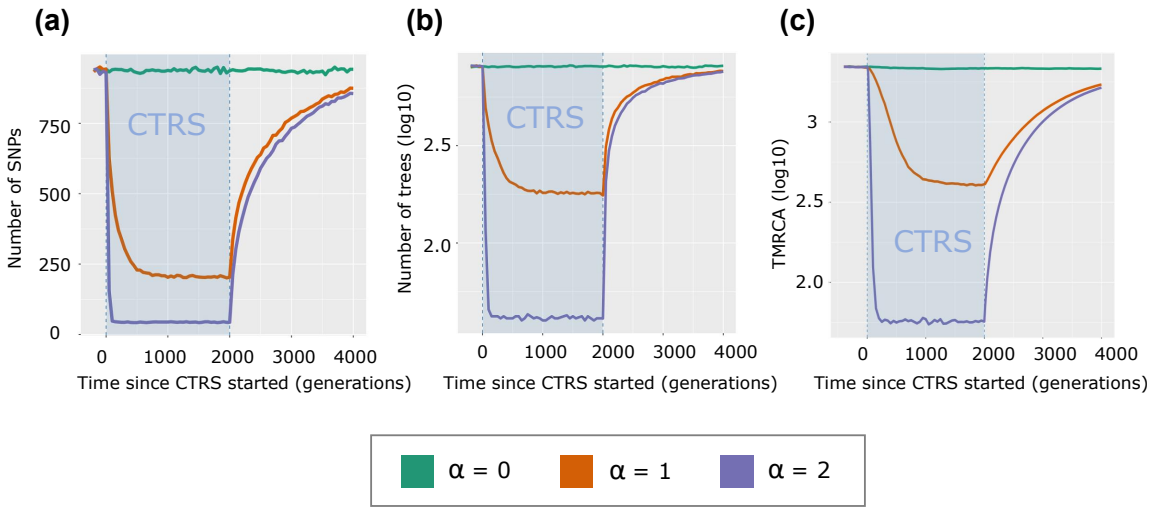

Figure S2: Number of SNPs (a), number of trees (log 10 scale) (b), and TMRCA (log 10 scale) (c) across generations. In all cases, the $b = 1$ model of variance in progeny size is used.

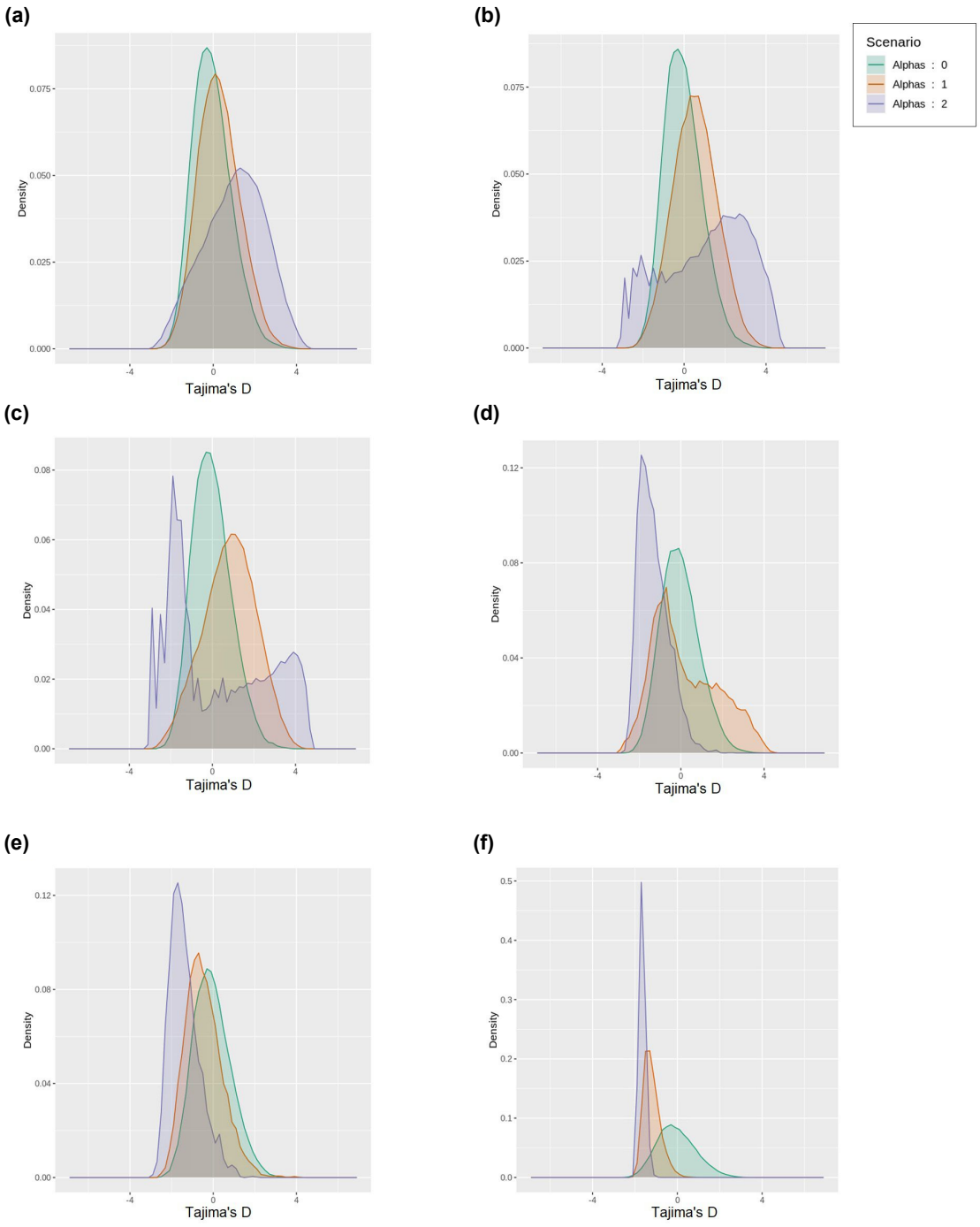

Figure S3: Distribution of Tajima's D across the genome. (a-e) 10, 20, 50, 500, 1500 generations since the starting of CTRS. (f) 500 generations without CTRS, after a period of 2000 generations of CTRS. The $b = 1$ model of variance in progeny size is used.

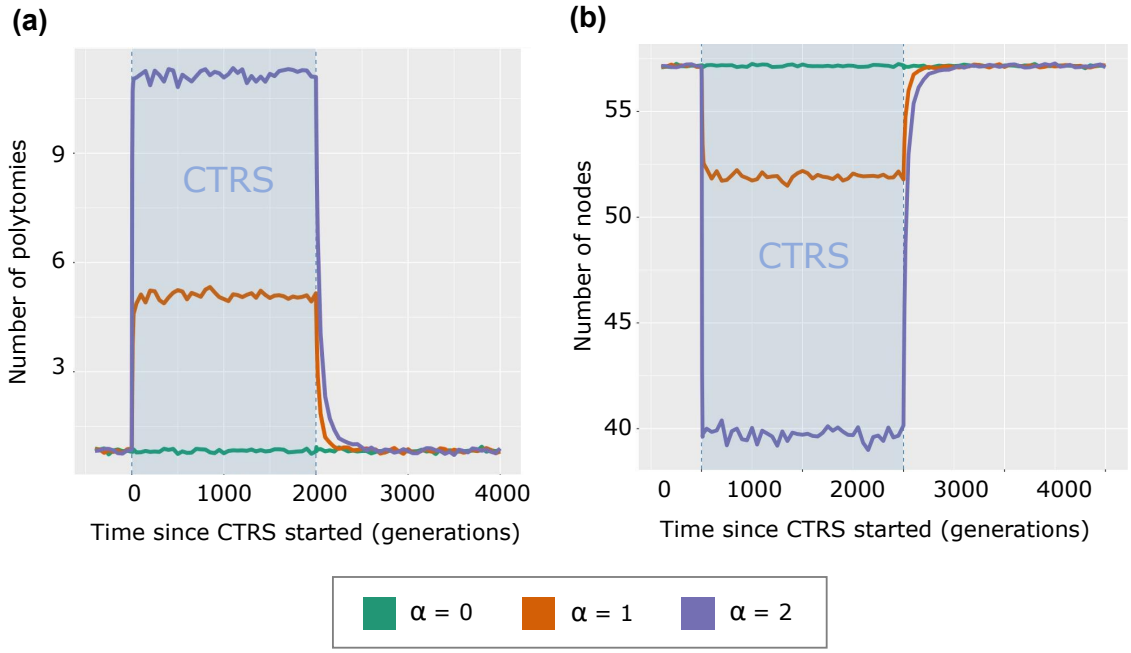

Figure S4: Number of polytomies (a) and number of nodes (b) throughout generations. The $b = 1$ model of variance in progeny size is used.

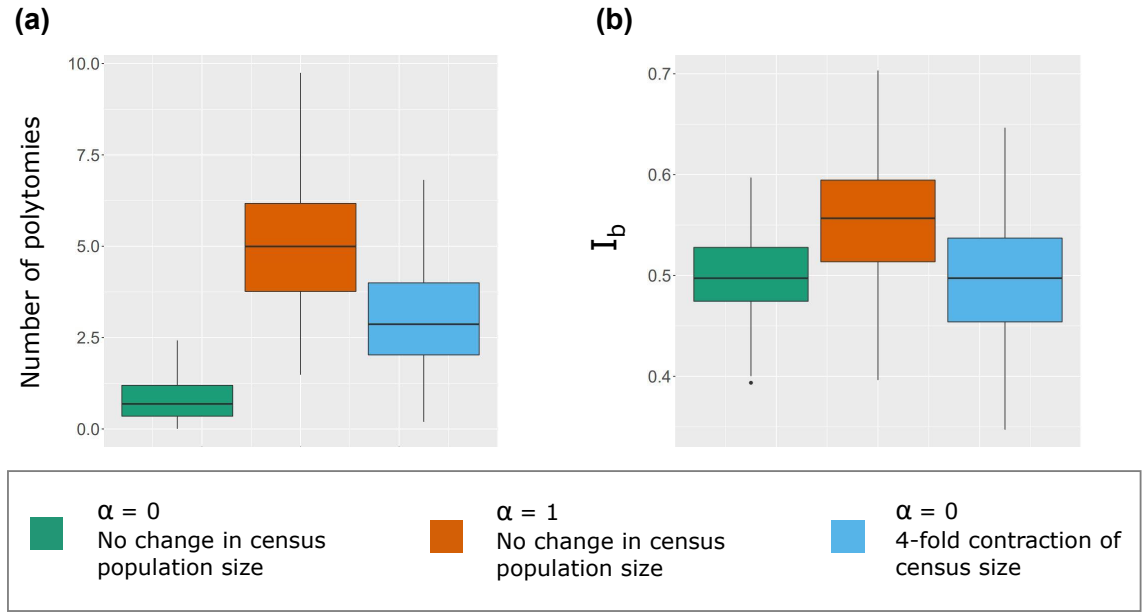

Figure S5: I_b and average number of polytomies for three scenarios. The CTRS in the $\alpha = 1$ scenario lasted for 500 generations before present. The 4-fold contraction happened 500 generations before present. In all cases, the $b = 1$ model of variance in progeny size is used.

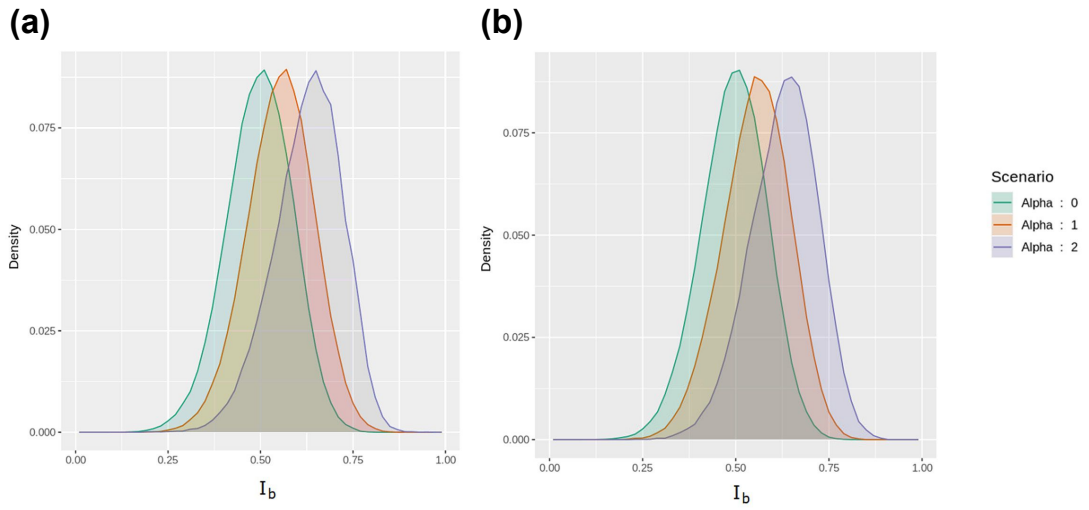

Figure S6: I_b distributions across the genome for $\alpha = 0$, 1, and 2, after 20 (a) and 500 (b) generations of CTRS. The $b = 1$ model of variance in progeny size is used.

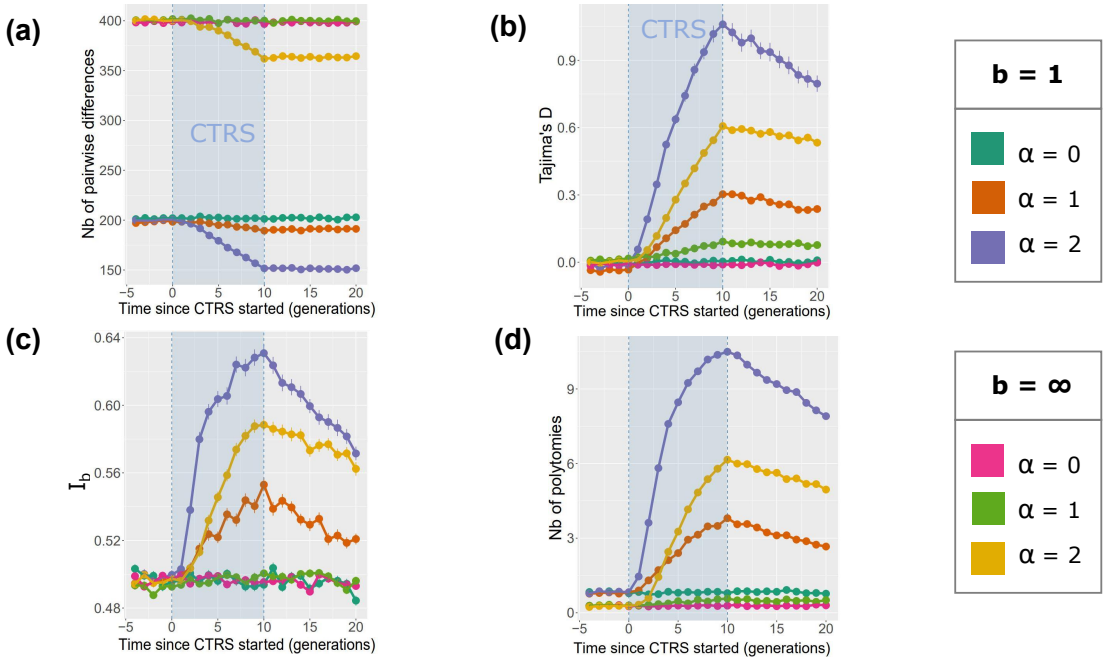

Figure S7: Number of pairwises differences, Tajima's D, number of polytomies and I_b under 10 generations of CTRS followed by 10 generations without CTRS. Both $b = 1$ and $b = \infty$ models of variance in progeny size are used.

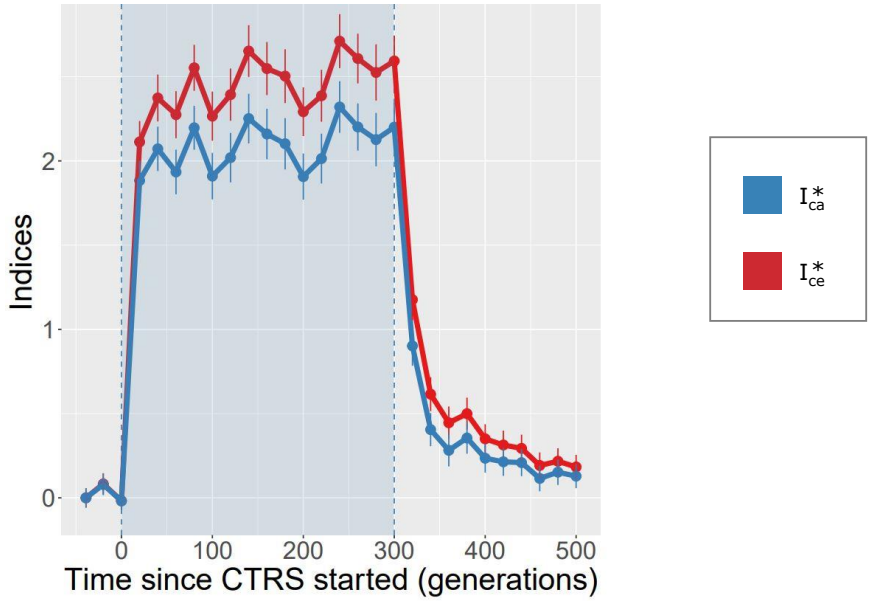

Figure S8: Two Colless index modifications to handle polytomies: I^*_{ca} and I^*_{ce}. See Methods for details on algorithms.

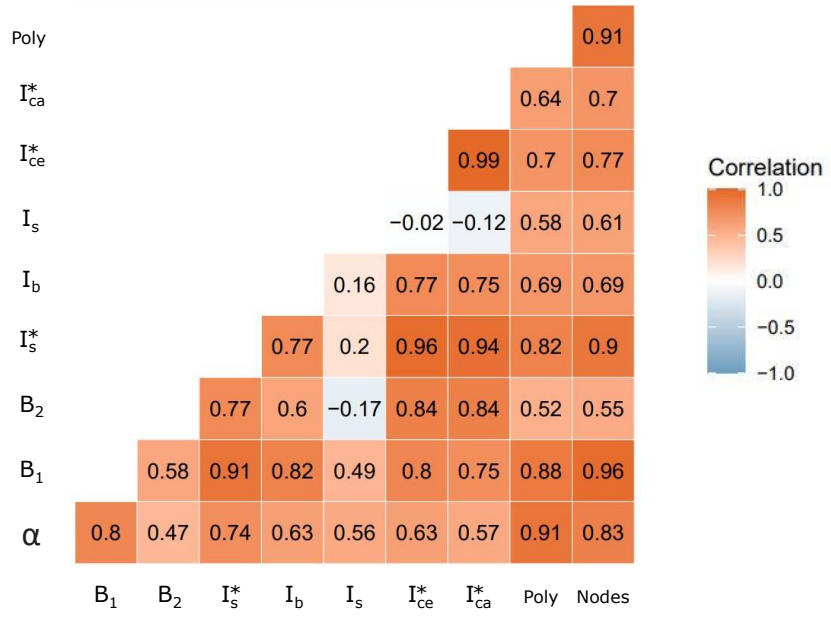

Figure S9: correlations between indices after 50 generations of CTRS.

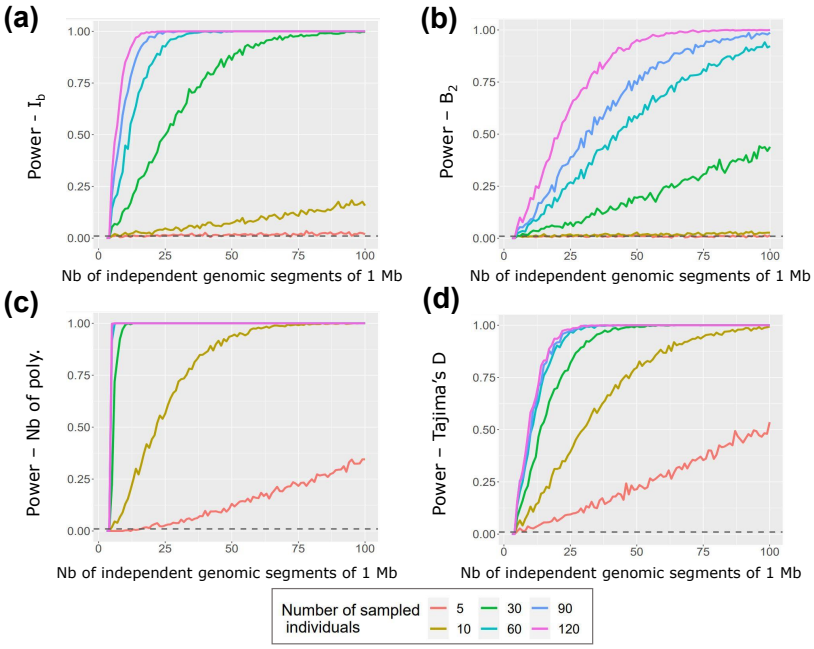

Figure S10: Power of distinguishing $\alpha = 1$ from $\alpha = 0$ scenarios (using a Wilcoxon test with the significance threshold set to 0.01), for 4 indices: I_b (a), B_2 (b), number of polytomies (c), Tajima's D (d).